#### **NURETH14-124**

# MEASUREMENT OF POST DRYOUT HEAT TRANSFER COEFFICIENT IN A DOUBLE HEATED ANNULUS WITH FLOW OBSTACLES

# I.Anghel, H. Anglart and S.Hedberg

Royal Institute of Technology (KTH), Stockholm, Sweden <u>iganghel@kth.se</u>, <u>henryk@kth.se</u>, <u>stellan@energy.kth.se</u>

#### **Abstract**

An experimental study on post dryout heat transfer regime in annuli with flow obstacles was conducted in the High-pressure Water Test (HWAT) loop at the Royal Institute of Technology in Stockholm, Sweden. The experimental investigations were performed in a wide range of the operational conditions: mass flux (500-750) kg/(m²s), inlet subcooling (10-40) K and system pressure (5-7) MPa. The wall superheat was measured at 88 different axial and azimuthal positions (40 on the inner tube and 48 on the outer tube). The results show an enhancement of heat transfer downstream of flow obstacles. The biggest influence has been observed in case of pin spacers and grid obstacle. This result is consistent with blockage area of various obstacles, which was the highest in case of pin spacers.

**Keywords:** Post-dryout, dryout, flow obstacles, heat transfer coefficient, annulus, measurements.

#### Introduction

The forced convective flow systems such as steam generators, cryogenic systems, spray cooling and nuclear reactors can experience an abnormal behavior where boiling crisis occurs and heated surface doesn't support anymore continuous liquid contact,[1]. This type of heat transfer regime is denoted as post-dryout heat transfer regime. It mainly occurs during force flow evaporation process when liquid film becomes depleted at the heated wall surface. During post dryout heat transfer regime, the heat is transferred mainly to the vapor. Therefore, the heat transfer coefficient is much lower with results of a dramatically increase of the wall surface temperature, [2].

A major influence on the post dryout heat transfer regime is exercised by the presence of the flow obstacles. One of the important objectives of the flow obstacle presence is to improve the heat transfer coefficient in the post-dryout region [3]. Recent studies indicated that the heat transfer coefficients can be increased as much as 120% for various types of flow obstacles, [3],[4].

The present work is a continuation of the experiments conducted at KTH in 2007, [5]. In this regard a new set of experiments with a significant improvement of the accuracy of the temperature measurements were carried out in 2010, [6]. The effects of three different kinds of flow obstacles have been investigated in an annulus with both, outer tube and inner tube walls heated.

The purpose of the study was to provide experimental data needed for validation of post-dryout heat-transfer models and, in particular, to study the effect of the flow obstacles on post-dryout heat transfer.

# The 14<sup>th</sup> International Topical Meeting on Nuclear Reactor Thermalhydraulics, NURETH-14 Toronto, Ontario, Canada, September 25-30, 2011

The other goal was related-in case of boiling water reactors (BWR), to understand the thermal and hydrodynamic processes due to the flow obstacles with a direct consequence in the thermal margins evaluation. The current safety standards stipulate that a nuclear reactor under normal operation conditions should have safety margins high enough to avoid the onset of dryout or Departure from Nucleate Boiling (DNB). This is mainly due to the fact that heat transfer conditions beyond the onset of dryout or DNB are not well understood and predictions of clad and fuel temperatures are quite uncertain. Whereas post-DNB heat transfer is very poor and typically lead to an immediate damage of the heater, post-dryout heat transfer can be quite efficient, and a damage of the heater can be avoided. This opens a new perspective towards the definition of the safety margin as a margin to the clad damage rather than a margin to the occurrence of dryout.

## 1. Experimental facility

#### 1.1 High-pressure Water Test loop

The post-dryout heat transfer experiments presented in this paper have been conducted in the in the High-pressure WAter Test (HWAT) loop at the Royal Institute of Technology in Stockholm, Sweden. The experimental facility consists of a main loop designed for the experimental part, a secondary circuit with coolant water at 20 °C used to cool the circulation pump and an electrical power supply.

The flow diagram of the main loop is shown in Figure 1. The loop was designed to operate at pressures up to 25 MPa and temperatures of the working fluid up to 340 °C. All parts in contact with water (except the test section) are made of stainless steel. A test section with length up to 7.5 m can be accommodated in the loop. An annulus which consists of two concentric tubes, with a length of 3.65 m was employed as the test section in the current experiments. The electrical power is supplied from a direct current generator. The maximum available magnitude for the current is 6600 A and voltages up to 140 V can be supplied.

The major components of the main loop are: filter, feed water pump, circulation pump, flow measurement system, control valve, pre-heater, test section, condenser and blow off valve. The instrumentation panel and the data acquisition system are located inside of the control room. During the operation, temperature and the pressure of the working fluid have to be monitored.

The loop is operating as follows. From the water supplier, the coolant has to pass first through a filter. After the filter, the water with an electrical conductivity less than 0.05 micro-Siemens is delivered to the main loop via the feed pump. The feed pump has a double role: to supply water to the loop and to increase the pressure to the desired value needed in the experiments. The circulation pump is used to maintain the flow within the main loop. During the experimental runs, the coolant can exhibit temperatures close to the saturation temperature. To avoid the cavitations phenomena, the temperature just upstream of the circulation pump is monitored continuously. The upper limit of the coolant temperature should not exceed 30 K bellow the saturation temperature. After the circulation pump, the coolant enters in a flow measurement system and continues further through the automatic flow controlling valve. The working fluid continues to flow through a heating system consisting of two serial pre-heaters. One of the pre-heater has a power of 155 kW and is needed to adjust the coolant inlet temperature to the conditions desired for the experimental run. Due to the length of the pipes between the pre-heater and the inlet of the test section, the heat losses through insulation are equivalent to 0.5-1.5 K in the temperature drop of the working fluid. To compensate heat losses a second pre-heater was installed just before the inlet to the test section. The temperature of the coolant is monitored upstream

of the measurement flow system, downstream of the pre-heater and at the inlet to the test section. From the test section, the coolant flows towards a condenser. The condenser has two distinctive circuits: a main circuit where the working fluid from the main loop condenses to single phase and a second circuit where the level of the cooling water is controlled using two automatically operated valves. The temperature of the cooling water is monitored continuously. The experimental facility is equipped with a blow-off valve with two main functions: to control the pressure in the system and to release the working fluid from the main loop in case of an emergency situation.

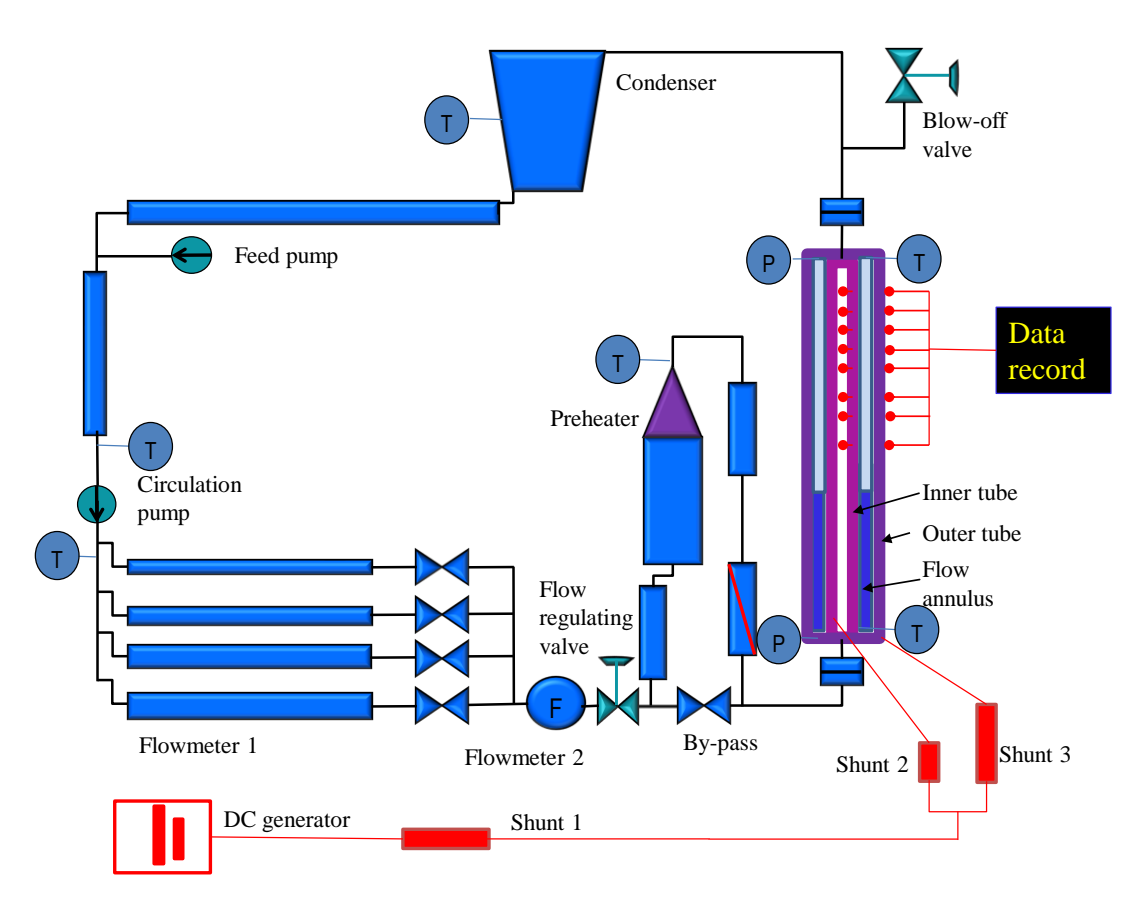


Figure 1 The High-pressure Water Test (HWAT) loop.

#### 1.2 Test section

The test section consists of an annulus assembled from two concentric tubes. In the present work the inner tube will be referred to as a **rod** while the outer tube will be referred to as a **tube**. Both, the rod and the tube are manufactured from Inconel 600. This material had been chosen because of the small rate of change of the resistivity with the temperature, [7]. The pipes are kept concentric by means of the five levels of pin spacers. The experiments were conducted in three different test sections: a test section with pins-spacer only denoted as **test section A**, a test section with pins-spacer and cylindrical obstacles denoted as **test section B**, a test section with pins-spacer and grid obstacles denoted as **test section C**.

The blockage area of the flow obstacles is: 10.13% in case of a pin spacer, 7.3% in case of a cylindrical obstacle and 10.07% in case of a grid obstacle. Figure 2 shows the three test sections used in the experiments.

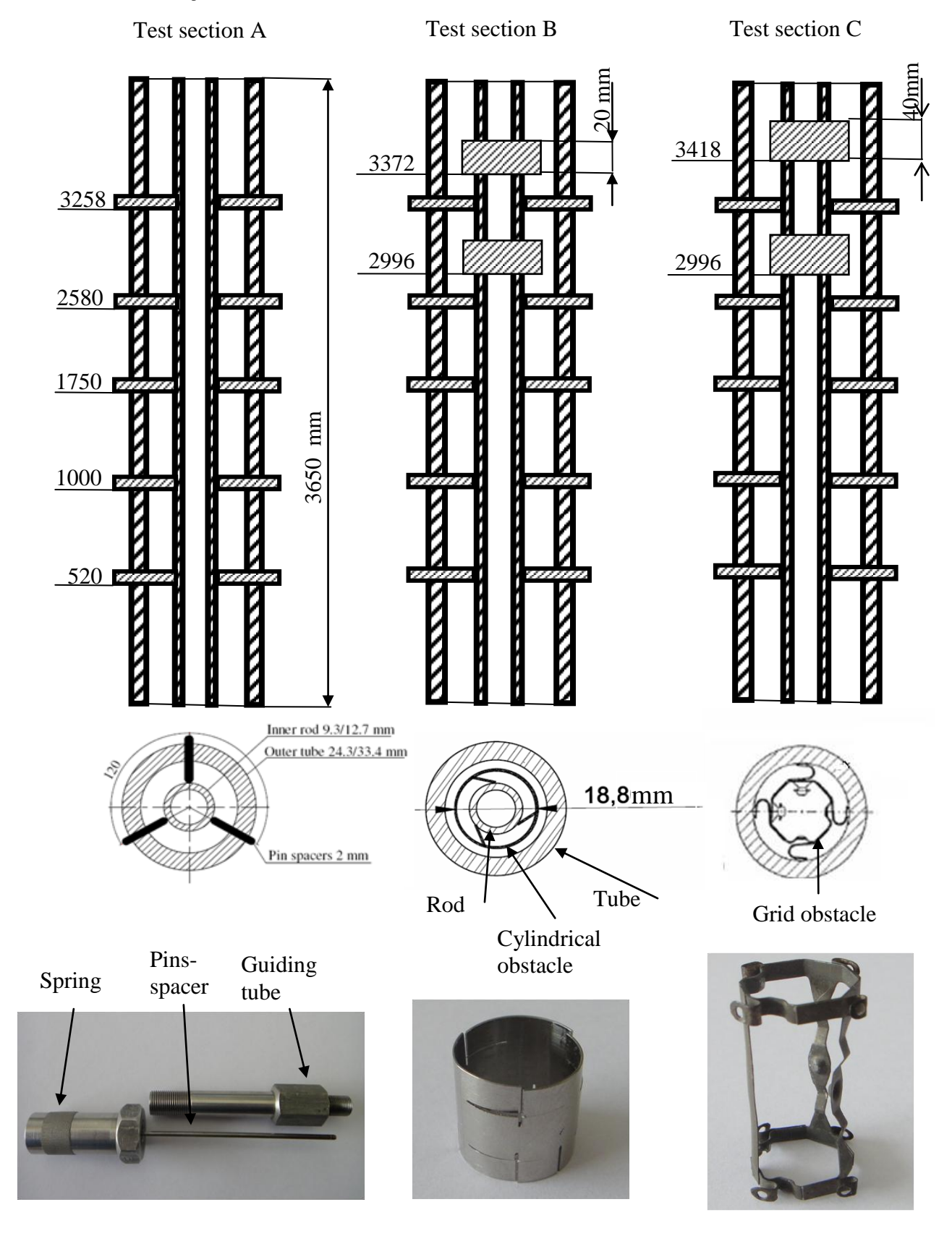


Figure 2 Test sections employed during experimental runs.

# 1.3 Temperature measurements

The temperature of the annulus walls were recorded with 80 K-type thermocouples, 40 located axially inside of the rod and 40 located outside of the tube. The thermocouples set inside of the rod were arranged in a bundle. One layer of a glass fibre tape and one layer of a mica tape were used to keep the bundle tightened. The layers of the tapes were used as well to insulate and to protect the thermocouple heads from the electrically conducting hot surface of the heated walls. The thermocouples set inside of the rod were pressed against the wall surface by small springs located in the opposite location on the diagonal. Axial locations of the thermocouples, which were equal to both the tube and the rod, are presented in Figure 3.

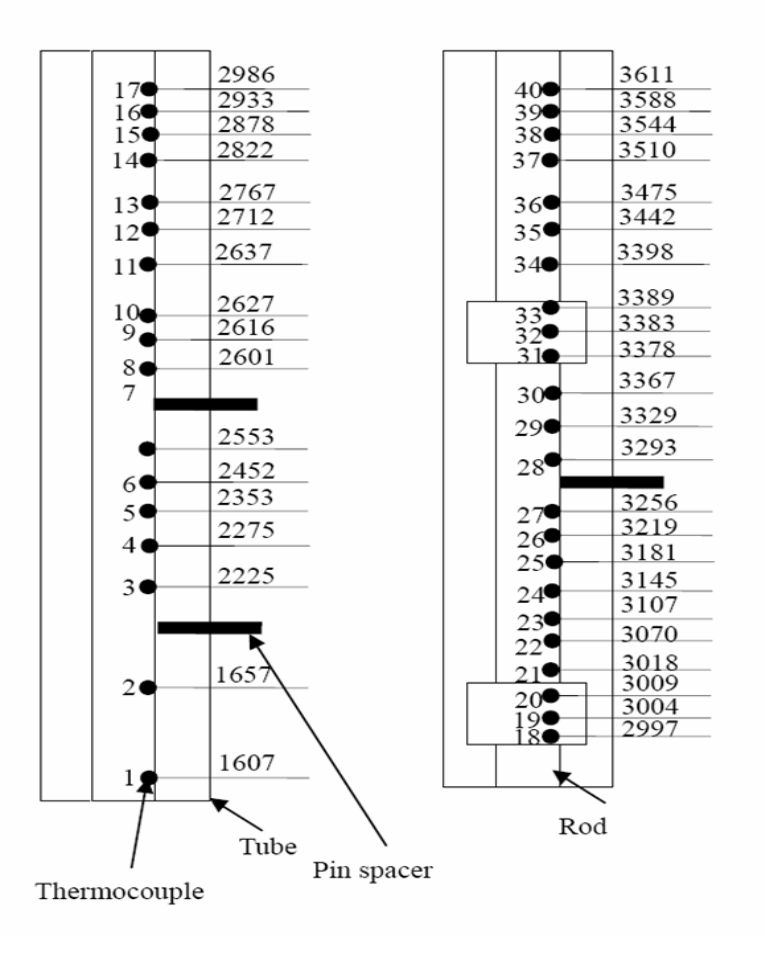


Figure 3. The thermocouples locations on the rod and tube walls (a distance from the beginning of the heated length in millimetres).

# 1.4 Experimental method

Experimental runs were initiated with single-phase runs in order to:

- measure pressure drop in the test section and obtain the friction coefficient
- relationship as well as an expression for local pressure losses for obstacles
- measure the inner and outer wall temperature at high Reynolds numbers to check the thermocouple readings and to validate the procedure to calculate temperature drop across the heated walls.

The standard methods to perform measurements of post-dryout heat transfer include the following steps:

- For a set of chosen parameters such as the inlet subcooling, the mass flux and the pressure, the power of the heater is set slightly below the level that corresponds to the first occurrence of dryout in the test section.
- Once the steady-state conditions were achieved, the power was increased step-wise (keeping the rest of the parameters constant) and the temperature distributions were recorded. First dryout occurrence was detected near the test section outlet.
- The procedure was repeated for the same inlet conditions, employing all three different kinds of flow obstacles.

During experimental runs the test section was uniformly heated, the ratio of the heat fluxes between rod and tube being one. No post dryout regime has been observed in case of the tube side during present experiments.

## 1.5 Uncertainty analysis

In the experimental studies, one of the most important issues is to evaluate the accuracy of measurements. The uncertainties in the present study can be classified as follow: uncertainty of a measured parameter, uncertainty of a derived variable due to the propagation of uncertainties of measured variables and uncertainty due to numerical iterations. All measurements of temperatures, pressure, pressure drops, mass flow rates, currents and voltages are subjects to an uncertainty degree.

- Uncertainty of temperature measurements is indicated for standard K thermocouples class 1 as: 1.5 K for a wall temperature up to 473 K and 2.5 K for a wall temperature up to 973 K, [8].
- Uncertainty of mass flow rate measurements:  $\pm 0.5$  %, [9].
- Uncertainty of static pressure measurements: ±0.01 %,
- During heat balance operation, the electrical power was compared with the enthalpy increase over the test section and the total power uncertainty was estimated as  $\pm 0.5$  %.

To correct the readings of the assembled thermocouples, three experiments were conducted in case of adiabatic, single phase flow at 299 K, 383 K and 483 K. An average of the inlet and outlet water temperatures, from the test section, which differs with less than 0.8 K was compared with the 40 thermocouple readings for the rod and 40 for the tube. For each case, a linear equation was established and extrapolated up till 850 K. The wall inner surface temperature of the rod and the wall outer surface temperature of the tube were corrected by adding temperature deviation,  $\Delta T$  to the measured values. The temperature corrections are presented in Figure 4.

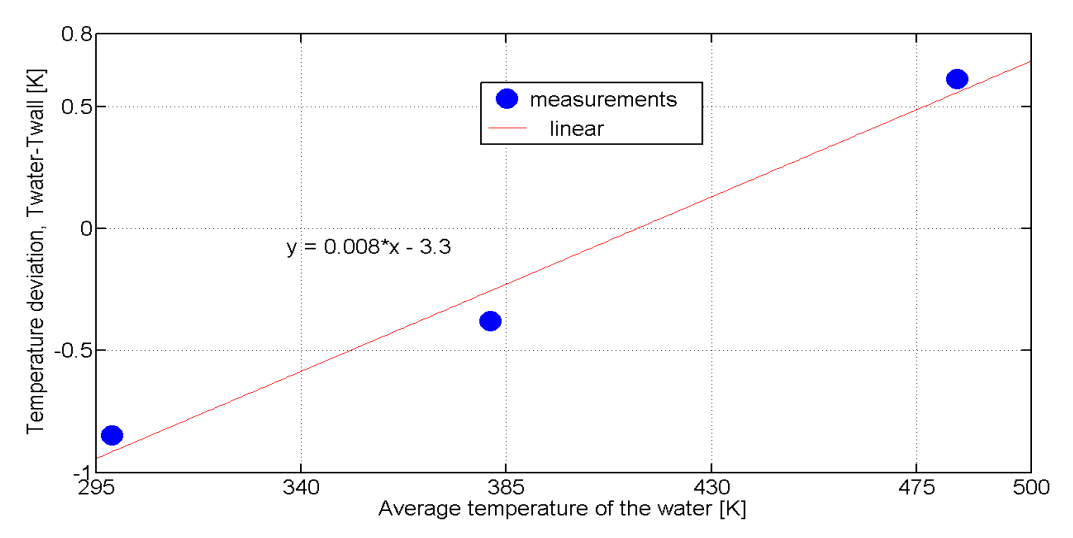


Figure 4 Temperature deviations for rod.

The outer wall temperature of the rod and the inner wall temperature of the tube are derived from the conduction equation with heat sources. The final forms for outer wall temperature of the rod and heat transfer coefficient are given in the following equations:

$$T_{ro} = T_{ri} + \frac{q_v}{2\lambda} \left( \frac{r_{ri}^2 - r_{ro}^2}{2} - r_{ri}^2 ln \frac{r_{ri}}{r_{ro}} \right) \tag{1}$$

$$h_{rod} = \frac{2\lambda \left[1 - \left(\frac{r_{ri}}{r_{ro}}\right)^{2}\right]}{r_{ro}\left[\frac{4\lambda \left(T_{ri} - T_{f}\right)}{q_{v}r_{ro}^{2}} + \left(\frac{r_{ri}}{r_{ro}}\right)^{2}\left(1 - 2ln\frac{r_{ri}}{r_{ro}}\right) - 1\right]}$$
(2)

$$h_{tube} = \frac{2\lambda \left[ 1 - \left( \frac{r_{ti}}{r_{to}} \right)^{2} \right]}{r_{ti} \left[ \frac{4\lambda \left( r_{to} - r_{f} \right)}{q_{v}r_{to}^{2}} + 1 - \left( \frac{r_{ti}}{r_{to}} \right)^{2} + 2ln \frac{r_{ti}}{r_{to}} \right]}$$
(3)

where,  $T_{ro}$ =wall temperature at the outer (wetted) surface,  $T_{ri}$ = wall temperature at the inner (insulated) surface,  $r_{ri}$ ,  $r_{ro}$ = the inner/outer radius of the rod,  $T_f$  = the fluid bulk temperature,  $q_v$ =volumetric heat density,  $T_{to}$ = wall temperature at the outer (insulated) surface of the tube,  $r_{ti}$ ,  $r_{to}$ = the inner/outer radius of the tube

The propagation error in case of the temperature of the rod outer wall and the heat transfer coefficient were found as:

$$u_{T_{ro}} = \left[ \left( u_{T_{ri}} \frac{\partial T_{ro}}{\partial T_{ri}} \right)^2 + \left( u_{q_v} \frac{\partial T_{ro}}{\partial q_v} \right)^2 + \left( u_{\lambda} \frac{\partial T_{ro}}{\partial \lambda} \right)^2 \right]^{1/2} \tag{4}$$

$$u_{h_{rod}} = \left[ \left( u_{T_{ri}} \frac{\partial h_{rod}}{\partial T_{ri}} \right)^2 + \left( u_{q_v} \frac{\partial h_{rod}}{\partial q_v} \right)^2 + \left( u_{\lambda} \frac{\partial h_{rod}}{\partial \lambda} \right)^2 + \left( u_{T_f} \frac{\partial h_{rod}}{\partial T_f} \right)^2 \right]^{1/2}$$
 (5)

where,  $u_{Tri}$ ,  $u_{Tfi}$  represent the temperatures uncertainties,  $u_{qv}$  represents the heat source uncertainty,  $u_{\lambda}$  represents the thermal conductivity uncertainty,  $u_{Tro}$ ,  $u_{hrod}$  represent the calculated uncertainties for the rod outer wall surface and heat transfer coefficient, respectively.

It can be easily seen that the influence of the heat flux and thermal conductivity is rather small in case of the wetted wall temperature calculation. The major source of uncertainty remains the precision of the thermocouples. As a consequence the uncertainty in calculation of the temperature of the outer wall of the rod is in a range of (1 to 2.5) K. In case of heat transfer coefficient, an additional source of uncertainty is represented by the temperature of the fluid.

Because the temperature of the outer wall of the rod and the temperature of the fluid are close to each other in the pre-dryout regime, the errors in heat transfer coefficient calculations exceed 30%. However the superheat in case of the post-dryout regime is several times higher than in the pre-dryout regime. Consequently, the error in calculation of the heat transfer coefficient is less than 1.5%. Figure 5 shows the errors bars for the heat transfer coefficient in case of a reference case.

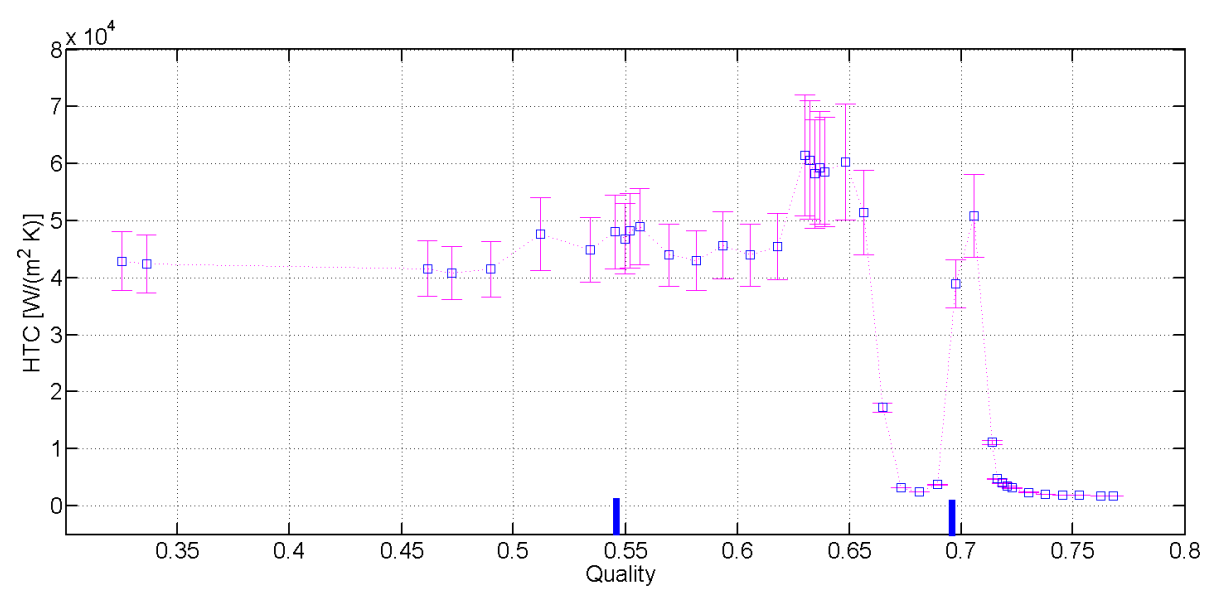


Figure 5 Measured heat transfer coefficient of the rod wall surface. Mass flux G=500 kg/m<sup>2</sup>s, inlet subcoolig  $\Delta T=10$  K, pressure P= 5 MPa.

#### 2. Results and discussion

## 2.1 The flow obstacle effect on the walls surface temperature

Figure 6 shows a comparison between the superheat of the rod surfaces for three different runs: test sections A, B and C. The inlet conditions are the same in all three cases, including the applied heat fluxes.

For the reference case (**test section A**) it can be observed that two dry patches developed upstream and downstream of the last pin spacer. The effect of the pin spacer is clearly visible: downstream of its location the dry patch is quenched along a distance of nearly 80 millimetres. A similar behaviour was noticed for **test section B**, for which a small influence due to the cylindrical obstacle was observed. Firstly, the dryout initiation upstream of the pin spacer is delayed with approximately 50 mm. The second dry-patch is delayed also over a distance equal with 100 millimetres. Secondly, at the dry-patch locations, the maximum temperatures of the wall surface were 50 K lower compared with the temperatures measured for the reference case.

The third line (triangles) shows the wall superheat for the run conducted in **test section** C. A slight peculiar dry-patch can be observed at the exit from the test section. Since blockage area of the grid obstacle is nearly equal to the one of the pin spacer, their effect is comparable. As a result the first grid obstacle cancels completely the dryout initiation downstream of its location, while the cylindrical obstacle only postpones the dryout occurrence. In case of the second grid obstacle the onset of dryout is delayed for a distance equal to 150 mm

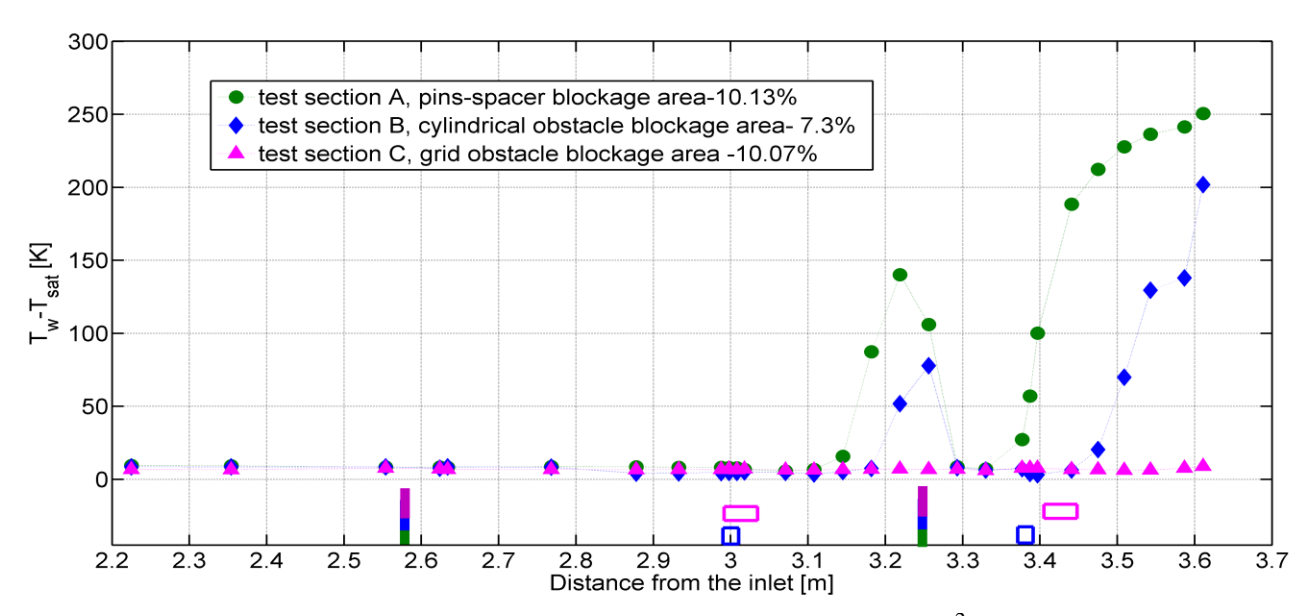


Figure 6 Measured superheat of rod wall surface. Mass flux G=500 kg/m<sup>2</sup>s, inlet subcoolig  $\Delta$ T=10 K, pressure P= 7 MPa, heat flux rod q''= 500 kW/m<sup>2</sup>.

# 2.2 The Heat Transfer Coefficient

In Figures 7 through 10 the heat transfer coefficient versus quality for both, the rod and the tube are shown. The experimental results are compared with the Chen correlation [10], for pre-dryout, and the Groeneveld correlation [11], in case of post-dryout conditions, respectively. Each obstacle used induces a different behavior. However in the pre-dryout region the experimental results are subject to high uncertainties due to the close values of the wall temperature to the saturation temperature.

Figures 7 and 8 show the heat transfer coefficient in case of experimental runs with pin spacers only. The turbulence induced by the pin spacers causes an increase of the heat transfer coefficient downstream of the pin spacers. The droplets entrained into the vapor core are driven randomly to the rod and tube wall surfaces making the liquid film thicker on both sides.

An enhancement of the heat transfer upstream of the dry-patch initiation can be observed. In both cases (with low and high inlet subcooling) the heat transfer coefficient increases in those regions most probably due to the intensive evaporation of the liquid film. The other effect noticed was a delay in the onset of dryout in case of the higher subcooling. The heat transfer coefficient presents a deterioration compared with the values observed in pre-dryout regime. This behaviour could be an indication that the liquid film is nearly disrupted in that point. However, before the dry patch initiation the heat transfer coefficient presents values closed to the one observed in the forced convective regime, indicating that the liquid film was re-made, Figure 8.

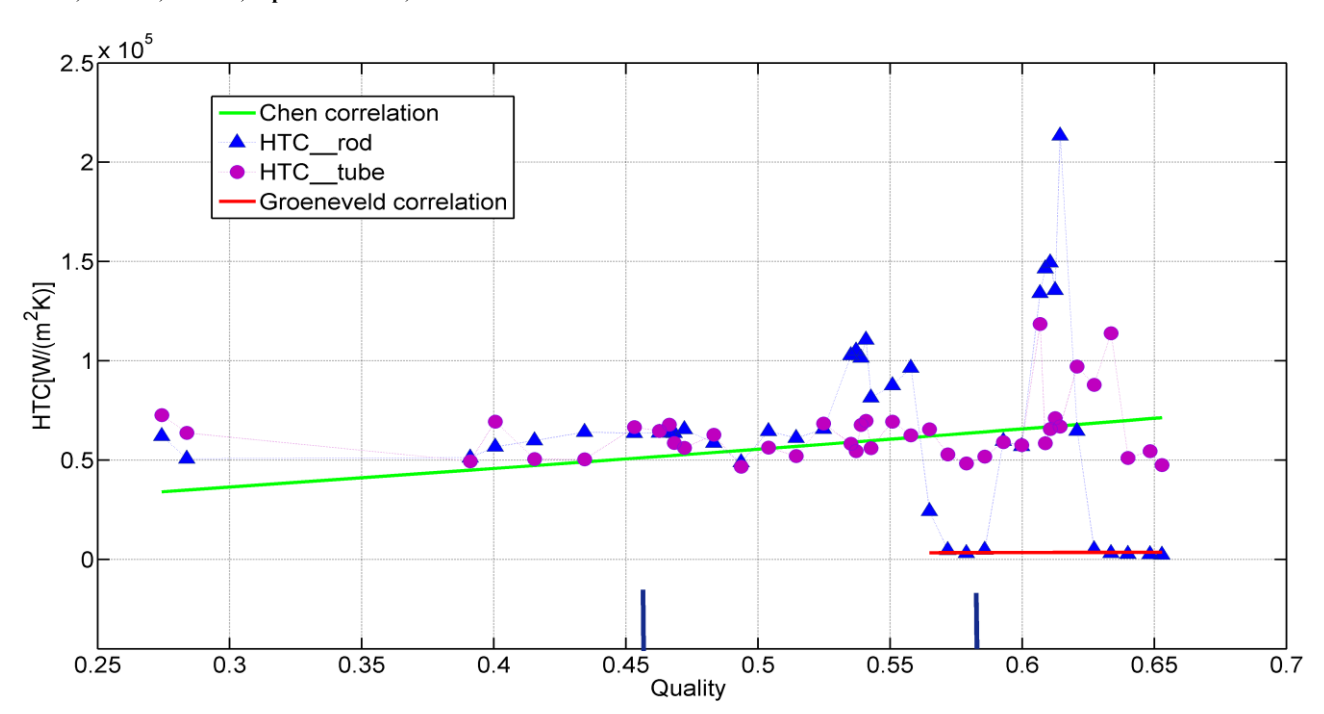


Figure 7 Measured heat transfer coefficient.. Mass flux G=750 kg/m<sup>2</sup>s, inlet subcoolig  $\Delta T$ =10 K, pressure P= 7 MPa, heat flux rod q''= 617.6 kW/m<sup>2</sup>, **test section A.** 

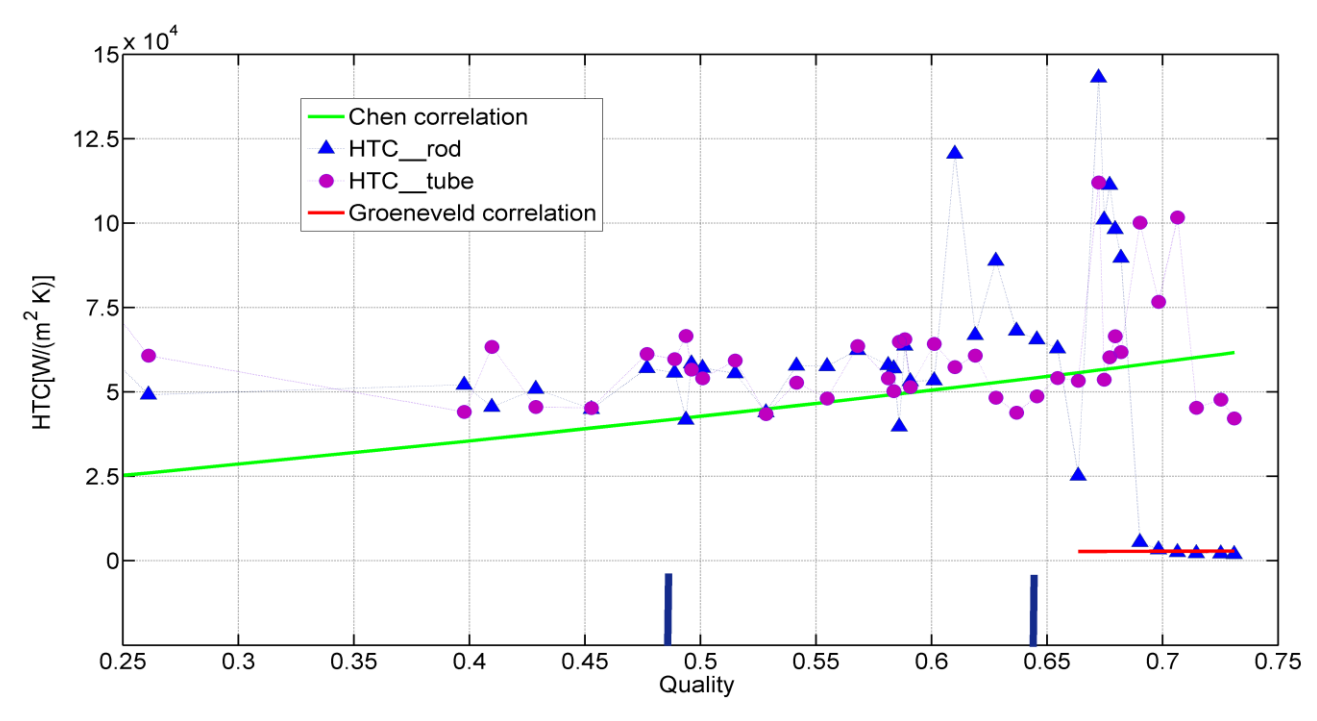


Figure 8 Measured heat transfer coefficient. Mass flux G=500 kg/m<sup>2</sup>s, inlet subcoolig  $\Delta$ T=40 K, pressure P= 7 MPa, heat flux rod q''= 566.9 kW/m<sup>2</sup>, **test section A.** 

The Chen correlation qualitatively agrees with the measured heat transfer coefficient downstream and upstream of the pin spacer locations. It can be observed a slight underestimation in case of higher subcooling for the rod case while on the tube side, downstream of the pin spacer locations fails to predict the heat transfer coefficient.

In the post dryout region a comparison with the Groeneveld correlation has been done. In both cases (lower and higher subcooling) the correlation is in agreement with the measured heat transfer coefficient. A very slight overestimation of the heat transfer coefficient in the post dryout region was observed. The immediate effect is an underestimation of the wall superheat.

Figures 9 and 10 show the heat transfer coefficient versus quality in case of experimental runs performed in **test sections B and C**. In both cases there are three respectively four dry patches developed for each of the runs. In both situations the pins spacers have the strongest effect, the regions downstream of the pin spacers being effectively quenched.

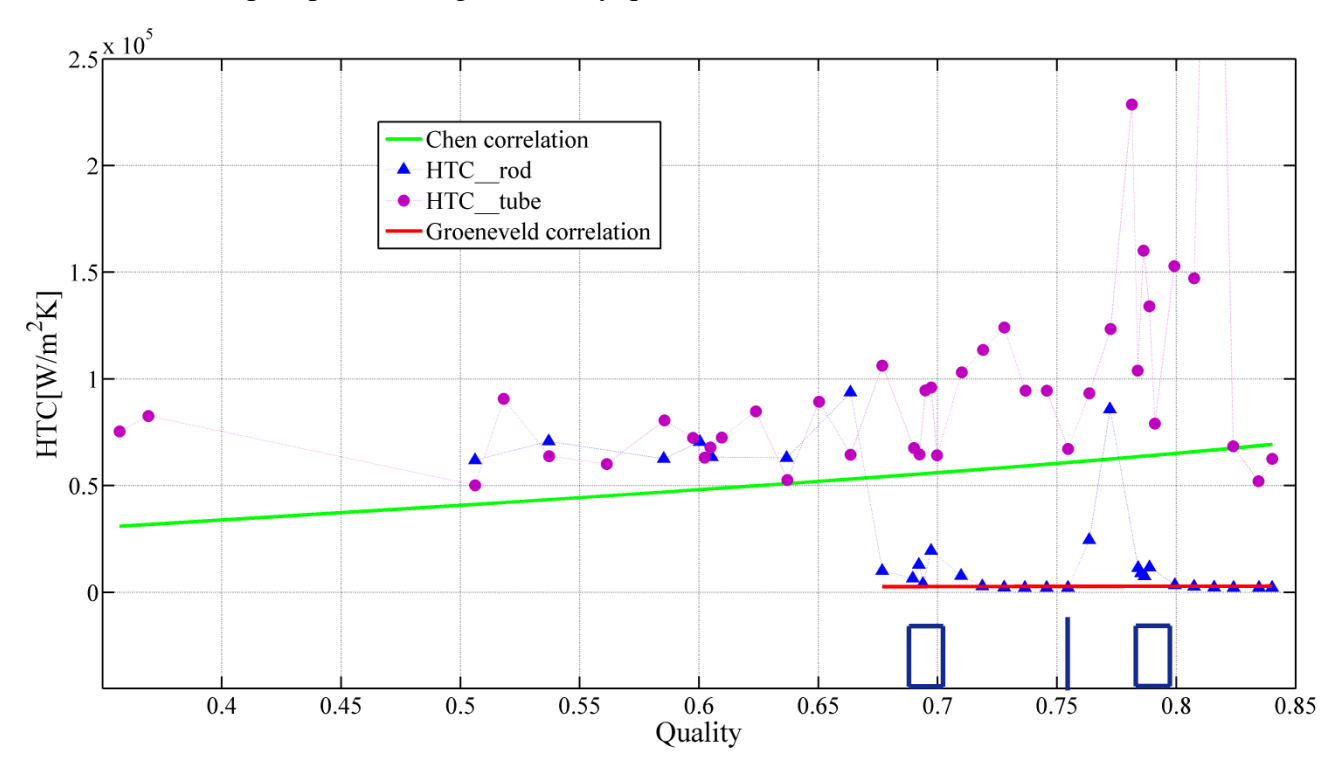


Figure 9 Measured heat transfer coefficient. Mass flux G=500 kg/m<sup>2</sup>s, inlet subcoolig  $\Delta T=10$  K, pressure P= 7 MPa, heat flux rod q''= 537.7 kW/m<sup>2</sup>, test section B.

The cylindrical obstacle, due to its blockage area, has a negligible influence on the post dryout heat transfer regime in case of the wall surface of the rod. The heat transfer coefficient is definetly increased at the cylindrical obstacle location but remains below the value corresponding to the forced convective boiling regime. The effect of the obstacle is immediately canceled downstream of its position, in case of the rod wall surface. Instead, the heat transfer coefficient is incressed on the wall surface of the tube, due to the turbulence induced by the cylindrical obstacle. The Groeneveld correlation presents a good agreement with the experimental data in case of experimental runs performed in **test section B**.

In **test section** C, the cylindrical obstacles were replaced with the grid obstacles. In order to capture the effect of the pin spacers, the second grid obstacle was shifted with 0.046 m towards the exit of the test section. Figure 10 shows the heat transfer coefficient obtained in an experimental run in which four dry patches were present. Three facts can be noticed: (a) the heat transfer coefficient downstream of the first grid obstacle location is improved to the values observed in the pre-dryout region,(b) a significant influence of the pin spacer leads to an enhanced heat transfer downstream its location (c) the combined

effect of the first grid obstacle and the pinspacer suggests a transition zone whereas the heat transfer coefficient presents lower values compared with the pre-dryout region but slightly higher compared with values observed in the mist flow regime.

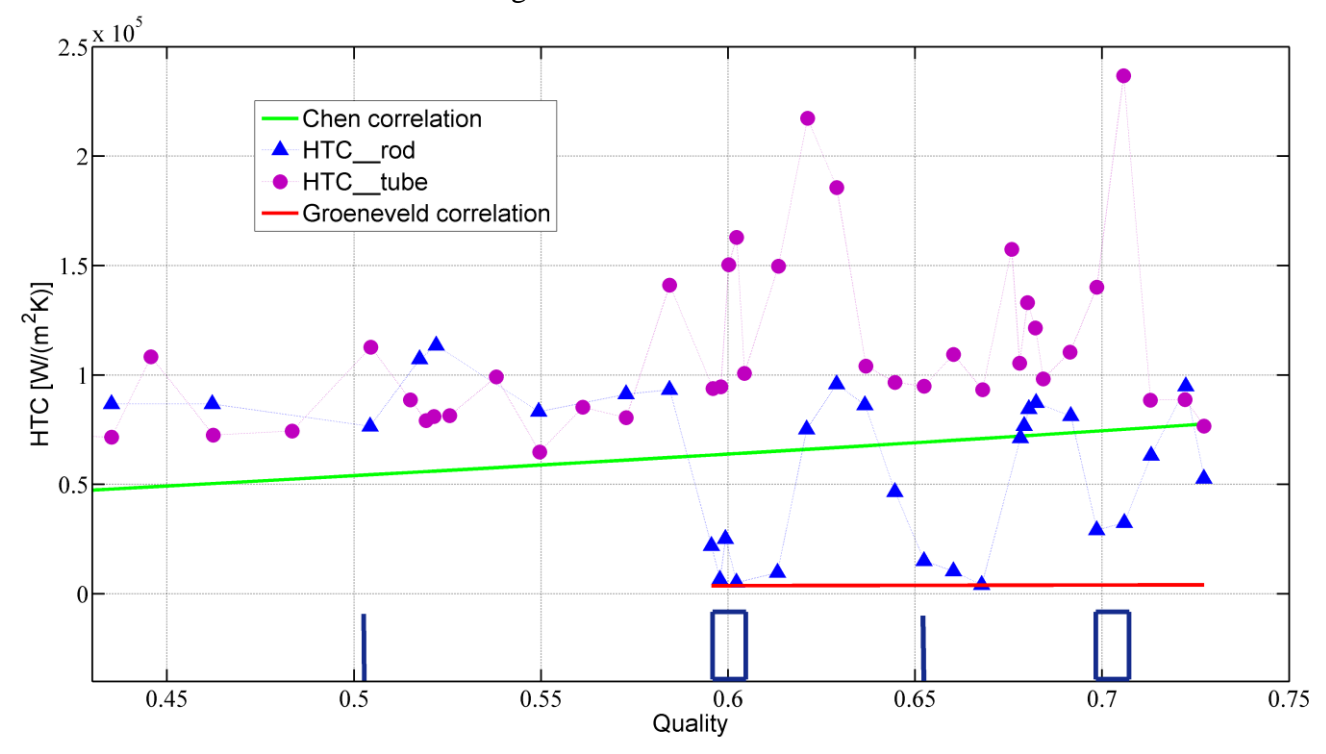


Figure 10 Measured heat transfer coefficient. Mass flux G=750 kg/m<sup>2</sup>s, inlet subcoolig  $\Delta T=10$  K, pressure P= 7 MPa, heat flux rod q''= 700 kW/m<sup>2</sup> test section C.

The Chen correlation is in agreement with the trend of the measured data but it underestimates the heat transfer coefficient in the pre-dryout heat transfer regime. The discrepancies are significant in case of the runs with pin spacers and grid obstacles. The reason can be the validity of the Chen correlation (valid for pressure below 3.9 MPa in the original version and below 6.9 MPa in the General Electric version).

#### **3 Conclusions**

It has been observed that the flow obstacles have an essential influence on the post-dryout heat transfer. From all three different kinds of flow obstacles, namely, pin spacers, cylindrical obstacles and grid obstacles, the pin spacers are the most effective ones (due to their highest blockage area from all investigated flow obstacles), even in the case of very high heat flux being able to influence the recovery of the liquid film downstream of their locations.

The heat transfer coefficient presents large uncertainties (over 30%) in the pre-dryout heat transfer regime. However, the uncertainties are low (about 2%) in the post-dryout heat transfer regime. In this regard the present data can be used for validation of mechanistic, high accuracy post-dryout heat transfer models.

A general agreement of selected correlation with the present data is satisfactory. However, it has been noticed that the Chen correlation under-predicts the heat transfer coefficient in the pre-dryout region, in

the direct proximity of the onset of dryout point. At this location heat transfer seems to be intensified due to increased evaporation of the liquid film.

#### 4 References

- [1] Groeneveld D.C, Delorme G., 1976, "Prediction of thermal non-equilibrium in the post-dryout regime," Nuclear Engineering and Design, **36**(1), pp. 17-26.
- [2] Hewitt G. F., Delhaye J. M., and Zuber N., 1992, Post-dryout heat transfer, CRC Press.
- [3] Pioro I. L., Groeneveld D. C., Doerffer S. S., Guo Y., Cheng S. C., and Vasic A., 2002, "Effects of flow obstacles on the critical heat flux in a vertical tube cooled with upward flow of R-134a," International Journal of Heat and Mass Transfer, 45(22), pp. 4417-4433.
- [4] Peng S., 2003, "Effects of flow obstacles on film boiling heat transfer," Nuclear Engineering and Design, **222**(1), pp. 89-95.
- [5] Anglart H., and Persson P., 2007, "Experimental investigation of post-dryout heat transfer in annulus with spacers," International Journal of Multiphase Flow, **33**(8), pp. 809-821.
- [6] Anghel I.G., Anglart H., Hedberg S., 2010, "Study of Post Dryout Heat Transfer in Annulus With Flow Obstacles," Proc. 14th International Heat transfer Conference, (IHTC14-22894).
- [7] Inconel 600 detailed technical report. http://www.haraldpihl.se/engelsk/index.html.
- [8] Omega Inc., Thermocouples guides http://www.omega.co.uk/guides/Thermocouples.html.
- [9] Flow Technology Inc, CA03-User manual.
- [10] Chen J.C., A correlation for boiling heat transfer to saturated fluid in convective flow, ASME Paper, 63-HT-34 (1963).
- [11] Groeneveld D.C., 1973. Post-dryout heat transfer et reactor operating conditions. Report AECL-4513.